Prospects for Bose-Einstein condensation of metastable neon atoms

H. C. W. Beijerinck, E. J. D. Vredenbregt, R. J. W. Stas, M. R. Doery, and J. G. C. Tempelaars

Physics Department, Eindhoven University of Technology, P.O. Box 513, 5600 MB Eindhoven, The Netherlands

The calculated upper limit $\mathcal{K}_i^{pol} \leq 10^{-14}$ cm^3/s of the rate constant for suppressed ionization in a gas of metastable Ne($^3P_2$) atoms in the fully aligned $|J=2, m_J=2\rangle$ state is used as input to investigate the prospects for achieving Bose-Einstein condensation (BEC). The heating rate of the trap population by secondary collisions of the hot products of the process of ionization—i.e., ground-state atoms, ions, and dimer-ions—with cold trapped metastable atoms is discussed in terms of a semiclassical model. An important step lies in limiting the depth of the magnetic trap to a value of a few millikelvin, to limit the range of small-angle scattering that contributes to heating. Also, a tight radial confinement reduces the probability for secondary collisions. At a trap depth of 10 mK, a radial dimension of 3 μm, and a density of 2×10^{13} cm^{-3} the heating rate is 1.4 μK/s, which should be compared to the transition temperature to BEC of 0.6 μK. The collisional heating is dominated by ion—metastable-atom collisions, due to their long-range charge-induced dipole interaction. Keeping the evaporative cooling switched on at $T=T_C$ reduces the heating a hundredfold. Using a bright beam of laser cooled neon atoms, an initial population of $\geq 10^{10}$ atoms can be loaded into a magneto-optical trap in one second. Tight magnetic traps are easy to achieve for metastable neon atoms, due to their magnetic moment of 3 μ_B. We conclude that achieving BEC is feasible for metastable neon. This also holds for triplet metastable helium, once the loading rate of traps has been improved. Finally, the semiclassical model used for calculating the heating rate is applicable to a wide range of inelastic collisions in trapped alkali gases and/or collisions with background gas.

PACS number(s): 03.75.Fi, 34.50.Fa, 05.30.$-$d, 51.90.$+$r

I. INTRODUCTION

Bose-Einstein condensation occurs when the mean interatomic distance becomes of the same order as the thermal De Broglie wavelength of the atoms, with the transition temperature T_C defined by the condition

$$\mathcal{D} = n\Lambda^3 = n(2\pi\hbar^2/mk_BT_C)^{3/2} = 2.61. \tag{1}$$

Here, $\mathcal{D}$ is the phase space density, n the number density, m the atomic mass, and k_B Boltzmann's constant. In 1995, Bose-Einstein Condensation (BEC) was first observed in a cold dilute sample of trapped alkali atoms, by three groups using Rb [1], Na [2], and Li [3], respectively. For temperatures below T_C, a macroscopic population of a single quantum state is obtained. Recently, in 1998 BEC was also achieved in a dilute gas of H atoms [4,5]. Since the first observation of BEC in a dilute gas, a whole new field of atom optics and coherent matter has emerged.

At this moment, most efforts in the field are still directed to Bose-Einstein condensation of the alkali atoms. Emphasis has been laid on Rb, the work horse in this new field, with Na as the runner up. For Cs it is not clear if BEC can be reached, due to the recently found experimental evidence on large dipolar relaxation rates for the $|F, m_F\rangle = |4,4\rangle$ and $|3,3\rangle$ states. For potassium, the main interest lies in producing a trapped, quantum-degenerate Fermi gas.

The advantages of investigating the alkali atoms are paramount. First, because the alkali atoms are trapped in their ground state, vapor-cell atom traps can be applied for achieving high density samples. Dual-chamber schemes result in trapped samples of the order of 10^8 atoms, using a pulsed or continuous cycle and a loading time of a few seconds. An

atomic beam approach using a thermal source and a simple Zeeman slower results in even higher loading rates, of the order of 10^{10} atoms/s. Second, there is a large body of spectroscopic and collision data on the alkali dimers. This allows one to extract accurate information on the potential surfaces involved. Third, based on this information, detailed calculations have been performed on the scattering of (ultra)cold atoms, resulting in reliable information on the scattering length. Also, the two- and three-body collisions that lead to the loss of atoms in the final magnetic trap, have been investigated. In most cases reliable rate constants for these loss processes are available; in some cases only lower or upper limits for these rate constants are available.

For the metastable rare-gas atoms the experimental conditions are less favorable. First, because the electronic energy of the metastable states is of the order of 8 eV (xenon) to 20 eV (helium), the relative population in a gas discharge or an atomic beam is only a fraction 10^{-4} or 10^{-5} of the total density. Therefore, techniques of beam brightening have to be used to obtain sufficiently large fluxes for loading atom traps. Second, the process of Penning ionization of two colliding metastable atoms is an important loss process. For an unpolarized sample, the rate constant is of the order of 10^{-10} cm^3/s [6–9]. In a spin-polarized sample, however, ionization is strongly suppressed by spin selection rules. For helium, theoretical estimates predict a suppression by a factor 10^4 to 10^5 [10,11]. This shows promise for trapping and evaporative cooling of metastable atoms in a magnetic trap [12,13]. For xenon, however, recent experiments show no evidence of suppression of ionization [8]: for a polarized sample the ionization rate is even larger by 50%. Third, the time scale for experiments is limited by the long but still finite lifetime of the metastable states. For triplet helium we
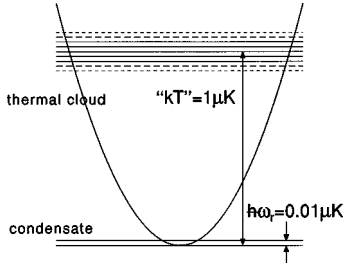
FIG. 1. Harmonic potential (with $\omega_z \ll \omega_r$) with a schematic view of the Bose condensate in the quantum mechanical ground state with energy $\hbar \omega_r$ [fraction $1 - (T/T_C)^3$] and the thermal cloud at temperature $T \gg \hbar \omega_r / k_B$ [fraction $(T/T_C)^3$]. In this schematic view the self-energy of the condensate has been neglected.

find $\tau = 9000$ s, which decreases to $\tau = 24$ s for neon [14] and $\tau = 43$ s for xenon [15] in the $^3P_2$ states. Finally, hardly any theoretical or experimental data on binary metastable atom collisions or interaction potentials are available [6,16] with He as an exception [9].

The outlook of a Bose-Einstein condensate of metastable rare gas atoms is promising enough to tackle all these difficulties. The idea of an atom laser of electronically excited atoms is tantalizing. Moreover, one can speculate on collective phenomena in a condensate with a large internal electronic energy, e.g., collective electronic deexcitation. Also, a condensate of metastable rare-gas atoms seems an ideal candidate for loading an optical lattice [17,18].

The advantages of using metastable rare-gas atoms are the excellent real-time diagnostics of the sample of trapped atoms, both in the stage of cooling above T_C as well as the stage below T_C where the condensate and the thermal cloud coexist (Fig. 1). Both the UV photons that are emitted when the metastable state decays as well as the ions produced in the still remaining ionizing collisions provide diagnostics for the density and the sample size. By combining this information with the geometry of the trapping field, we can also determine the temperature in a noninvasive way.

In this paper we investigate the feasibility of reaching conditions where Bose-Einstein condensation occurs for metastable neon. We have investigated two geometries of the sample in a magnetic trap, resulting in two different, cylindrically symmetric geometries of the final state condensate. First, a high density final state with a small aspect ratio is discussed, with the latter defined as the ratio of the long over the short axis of the ellipsoidally shaped thermal cloud of trapped atoms. Second, a low density final state with a very large aspect ratio is investigated. The former is close to the geometry used by the group of Ketterle for achieving BEC in sodium [19]; the latter corresponds to the geometry used for the recent BEC experiments with atomic hydrogen [4,5]. Typical values of the sample size, aspect ratio and number density are given in Table I for the two geometries, together with the transition temperature T_C.

To provide a reference frame for the disturbing effects of heating of the sample, we first discuss the creation of hot

TABLE I. Characteristic parameters for neon of the initial state of evaporative cooling and two final states in the magnetic trap at the onset of BEC. The count rate and decay time of the real time diagnostics are given for all three states.

Parameter	Initial state	Final state (high density)	Final state (low density)
radius (μm)		10	3
length (μm)		22	250
aspect ratio		1:2.2	1:83
population N (no. of atoms)	10^{10}	10^6	2×10^5
number density n (cm^{-3})	5×10^{11}	10^{14}	2×10^{13}
temperature T (μK)	2×10^3	1.7 [a]	0.6 [a]
phase space density	3.2×10^{-7}	2.61	2.61
rate constant $\mathcal{K}_{el}$ (10^{-12} cm^3 s^{-1})	2300 $(a_{2,2}/50a_0)^2$	6.6 $(a_{2,2}/50a_0)^2$	3.9 $(a_{2,2}/50a_0)^2$
"good-to-bad" ratio $n\mathcal{K}_{el}/(n\mathcal{K})_{gas}$ [b]	2260 $(a_{2,2}/50a_0)^2$		
"good-to-bad" ratio $\mathcal{K}_{el}/(\mathcal{K}_i^{pol})_{max}$		665 $(a_{2,2}/50a_0)^2$	389 $(a_{2,2}/50a_0)^2$
elastic collision rate $n\mathcal{K}_{el}$ (s^{-1})	113 $(a_{2,2}/50a_0)^2$	665 $(a_{2,2}/50a_0)^2$	78 $(a_{2,2}/50a_0)^2$
UV count rate S_{uv} (s^{-1})	2.8×10^5	33	7
ion count rate S_i (s^{-1})	5×10^7	1×10^6	4×10^4
probe ion count rate S_x (s^{-1}) [c]	4×10^8	8×10^6	3.2×10^5
UV decay time τ_{uv} (s)	24	24	24
ionization decay time τ_i (s)	200	1	5
probe decay time τ_x (ms)	25	0.125	0.625

[a]Equal to the transition temperature T_C.
[b]At a background pressure of 10^{-9} Torr.
[c]Exciting a fraction 10^{-3} of the total population.

(dimer-) ions and ground-state atoms by ionization in terms of an equivalent background pressure in the trapping chamber. This approach provides an easy comparison to experiments with alkali atoms, where background gas scattering is the dominant loss process at low densities of the trapped atoms. In this case, hot ground state atoms invade the trapped sample, causing an extra trap loss and an extra heating of the sample of trapped atoms. For this reason, in most alkali experiments, the evaporative cooling is not switched off after reaching BEC. For the two final state geometries (Table I) of our trapped metastable neon atoms, the ionization rate is equal to $\dot{N}_i = 10^6$ s^{-1} and $\dot{N}_i = 4 \times 10^4$ s^{-1} for the high-density and the low-density case, respectively. These rates correspond to an equivalent background pressure of 3×10^{-10} Torr and 3.6×10^{-12} Torr, respectively. This approach gives some feeling to what extent the condensate is disturbed by the hot products of residual ionization.
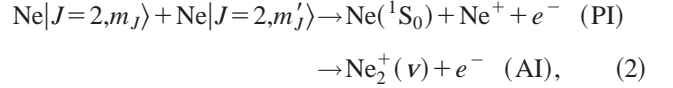
However, we have to keep in mind that these hot products consist of both (dimer) ions and atoms in the ground state [see Eq. (2)] with a wide range of collision energies, ranging from 2 to 125 K for the neon system. Both features have a major influence on the cross sections involved and the resulting influence on both particle loss and heating. For example, the (dimer) ion—metastable-atom interaction is dominated by the charge-induced dipole interaction with its long-range C_4/R^4 potential. Only a very careful, fully quantitative analysis of the collision processes involved can resolve the major question of this paper: can BEC be reached for metastable neon? Also, we want to identify the most favorable experimental conditions for achieving BEC. For comparison, we finally apply our thorough analysis to the case of triplet metastable helium to answer the same question of the feasibility of BEC.

In Sec. II, the suppression of ionization in a realistic situation of trapping and cooling is presented, based on the recent work by Doery *et al.* [6]. In Sec. III, we discuss the dynamics of the ionizing collisions to determine the energy released in the hot products. The heating of the sample by inelastic collisions and the recoil due to radiative decay is treated in Sec. IV. First, we present a semiclassical framework for accurately describing the heating rate of the sample by the secondary collisions of the hot products Ne($^1S_0$), Ne$^+$, and Ne$_2^+$ with trapped metastable neon atoms. Next, we apply the model to the case of metastable neon in Sec. V, which enables us to evaluate the advantages and disadvantages of the two final state geometries.

In Sec. VI we discuss the bright beam used for loading the atom trap. The dynamics of the process of evaporative cooling are also treated in this section, using the review papers by Walraven [20] and Van Druten and Ketterle [21] as a starting point. The diagnostics for the sample size and density are discussed in Sec. VII. In Sec. VIII we investigate the prospects for BEC in triplet metastable helium, again using the semiclassical model. Finally, in Sec. IX, we wrap up the paper with some concluding remarks. The main conclusion is that for both Ne* and He* the prospects for achieving BEC are good.

II. SUPPRESSION OF IONIZATION

The process of ionization [22] for a sample of metastable neon atoms in the $^3P_2$ state with an electronic energy of 16 eV is given by

$$\mathrm{Ne}|J=2,m_J\rangle + \mathrm{Ne}|J=2,m'_J\rangle \rightarrow \mathrm{Ne}(^1S_0) + \mathrm{Ne}^+ + e^- \quad (\mathrm{PI})$$
$$\rightarrow \mathrm{Ne}_2^+(v) + e^- \quad (\mathrm{AI}), \qquad (2)$$

with m_J indicating the magnetic substate. The kinetic energy of the electron is of the order of 12 eV, as determined by the difference potential of the initial and the final state. In the first reaction (Penning ionization, or PI), the final state neon ions and atoms in the ground state each carry a kinetic energy on the order of 100 to 500 K, depending on the energy gained in the well of the initial state potential and the internuclear distance where ionization occurs. In the second reaction path, usually referred to as associative ionization (AI), almost all of the initial state kinetic energy is stored in the molecular ion as vibrational energy. The kinetic energy of the molecular ion in the final state is due to the center-of-mass energy of the colliding Ne* atoms.

The dominant process leading to ionization is the *exchange* mechanism based on the Coulomb interaction of the electrons involved. In this case the valence electron of atom (1) transfers to the available core-state of atom (2), leaving the core of atom (1) to form a positive ion. The valence electron of atom (2) is no longer bound and leaves the scene [24–26]. The *radiative* mechanism is absent for these metastable atoms, because it requires the existence of a dipole-allowed transition to a lower state.

Because the Coulomb interaction does not affect the electron spin, the magnetic quantum number m_S of the total spin S does not change. For two atoms in a pure $|J=2,m_J=2\rangle$ state the process of ionization is spin forbidden. However, the anisotropic nature of the long-range electrostatic interaction due to the $(2p)^{-1}$ core hole will apply a torque that can rotate the total angular momentum J of the atoms with respect to each other. This will result in a residual ionization, even for initially fully aligned atoms [6].

Detailed quantum-mechanical calculations of the ionization rates for (ultra) cold collisions have very recently been performed by Doery *et al.* [6]. Both the electrostatic dipole-induced dipole $V_{DD} = -C_6/R^6$ and the quadrupole-quadrupole term $V_{QQ} = C_5/R^5$ (due to the core only) are included in the long range potentials. For the short range, information is derived from the $\mathrm{Na}_2(^3\Sigma_u^+)$ and $\mathrm{Na}_2(^1\Sigma_g^+)$ potentials. The results show that the anisotropy ΔC_5 in the quadrupole-quadrupole interaction (defined as the range of C_5 values found for the different molecular potentials, with $\langle C_5 \rangle = 0$) is the dominant driving force for the residual ionization (Fig. 2). Its influence exceeds the effect of the dipole-induced dipole term by a factor of 12. For neon, we find $\Delta C_5 = 0.84$ a.u. [6] and $\Delta C_6 = 4.5$ a.u. at $C_6 \approx 1952$ a.u. [6]. The rate constants $\mathcal{K}_i$ and $\mathcal{K}_i^{\mathrm{pol}}$ for the unpolarized and polarized case, respectively, are given by

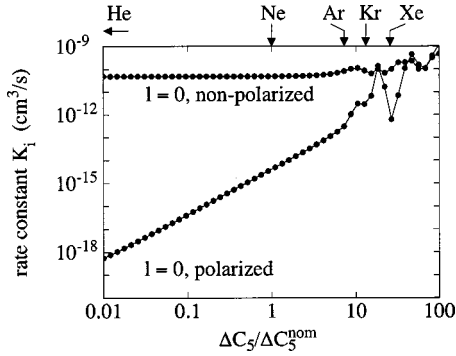$$\mathcal{K}_i = 8 \times 10^{-11} \text{ cm}^3/\text{s},$$

FIG. 2. Calculated ionization rate for both an unpolarized as well as a polarized sample of metastable rare gas atoms, as a function of the anisotropy $\Delta C_5 / \Delta C_5^{nom}$ due to the $(2p)^{-1}$ core hole. The parameter ΔC_5^{nom} is the value of ΔC_5 for neon. We observe a scaling $\mathcal{K}_i^{pol} \sim (\Delta C_5)^2$. The collision energy is $E = 1$ μK, where s-wave scattering with angular momentum $\lambda = 0$ occurs. The arrows indicate the value for Ar*, Kr*, and Xe*.

$$\mathcal{K}_i^{pol} = 5 \times 10^{-15} \text{ cm}^3/\text{s}. \tag{3}$$

For collison energies $E \lesssim 1$ mK, as relevant for trapping and cooling, these rate constants are energy independent.

Because resonances due to quasibound states can influence the ionization rate considerably, due to the longer collision times involved, Doery *et al.* [6] have varied the well depth of the Na$_2$ triplet potential which is dominant for the value of $\mathcal{K}_i^{pol}$. The results are given in Fig. 3 as a function of the semiclassical phase Φ of the Na$_2$ triplet potential for a range slightly larger than π radians, i.e., over at least one bound state. We observe a variation of the ionization rate $\mathcal{K}_i^{pol}$ for polarized atoms over more than three orders of magnitude. However, for the larger part ($\approx 98\%$) of the range in phase the ionization rate is less than

$$(\mathcal{K}_i^{pol})_{max} = 10^{-14} \text{ cm}^3/\text{s}, \tag{4}$$

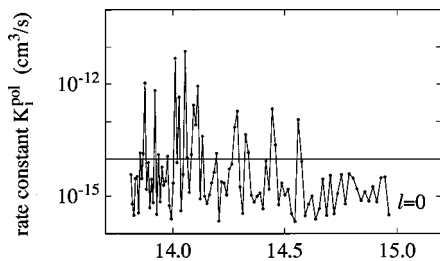which we will use throughout this paper to calculate the influence of the residual ionization in a trapped sample.

FIG. 3. Calculated residual ionization rate $\mathcal{K}_i^{pol}$ for Ne$|2,2\rangle$ + Ne$|2,2\rangle$ collisions as a function of the well size of the Na$_2$ triplet potential used to model the short-range interaction. The well size is measured in terms of the semiclassical phase $\Phi = \int_\rho^\infty [-2mV(R)/\hbar]^{1/2} dR$ with $V(\rho) = 0$ over a range slightly larger than π, i.e., over at least one vibrational state. This implies that we scan over all possible resonances. The collision energy is $E = 1$ μK, where s-wave scattering with angular momentum $\lambda = 0$ occurs.

When varying the phase of the Na$_2$ singlet potential, the value of $\mathcal{K}_i^{pol}$ never exceeds the upper limit of Eq. (4).

Of course, we should keep in mind that the treatment of Doery *et al.* [6] does not provide a final answer, in the sense that other mechanisms for spin-flips exist that have *not* been taken into account. For instance, at short range ($R < 10a_0$) orientation of the core of the metastable atoms could lead to a splitting among the nine possible spin-polarized potentials. A full theoretical treatment awaits the development of reliable *ab initio* short-range potentials, such as currently undertaken by Kotochigova *et al.* [23].

An effect of second order spin-orbit splitting, that turned out to be important for the heavier alkali atoms, is not to be expected for metastable neon atoms due to its scaling with Z^2 with Z the nuclear charge. Another process that has not been taken into account in the calculation of the residual ionization is the magnetic dipole-dipole interaction, which is the cause of residual ionizing collisions in a spin-polarized gas of triplet metastable helium atoms. However, the resulting rate constant for this process is roughly 10^{-14} cm^3 s^{-1} for this system, the same value as the upper limit for the rate constant which we use throughout this paper for investigating the role of residual ionization for metastable neon atoms.

On the other hand, the occurrence of a resonance might not be prohibitive at all for reaching the transition to BEC in metastable neon. First, one can always switch to the other abundant isotope ^{22}Ne. Second, resonances can be shifted by applying homogeneous magnetic fields. Thirdly, the occurrence of a resonance in the ionization rate constant is probably accompanied by an analogous resonance in the scattering length $a_{2,2}$. The ratio of "good-to-bad" collisions, which is the important number for effective evaporative cooling, is then not influenced and keeps the road to BEC quite open (Sec. VI D).

The definitive answer on the actual magnitude of the suppression of ionization in a spin-polarized gas of metastable neon atoms has to be provided by future experiments, by looking at the ion yield of a sample trapped in a magnetic trap (Sec. VII). The proof of the pudding is in the eating.

In Table I we present the ionization decay time for the two geometries investigated, resulting in $\tau_i = 1$ s and $\tau_i = 5$ s for the high density and low density case, respectively. Both decay times are much shorter than the finite lifetime $\tau_{uv} = 24$ s of the metastable state, i.e., ionization fully determines the time available for measurements in the final state.

III. ENERGY RELEASE IN IONIZING COLLISIONS

Once the rate constant for ionization has been determined in a quantum-mechanical calculation, the energy release can be described in fully semiclassical terms [22]. A schematic view of the initial and final state potentials of the process of Eq. (2) is given in Fig. 4. The energy of the electron is determined by the difference potential $|V^* - V^+|$, with V^* and V^+ the real potentials corresponding to the Ne* + Ne* initial state and Ne$^+$ + Ne($^1S_0$) final state, respectively. The imaginary part of the interaction potentials, the so-called auto-ionization width $\Gamma(R)$, is an exponentially decaying function with a characteristic length on the order of $2a_0$ [6].
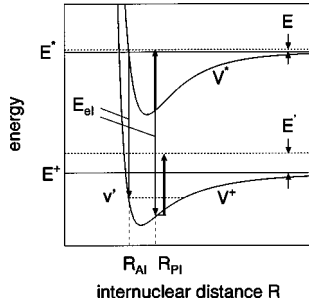
FIG. 4. Schematic view of the initial state $Ne|2,2\rangle + Ne|2,2\rangle$ potential $V^*(R)$ and the final state $Ne(^1S_0) + Ne^+$ potential $V^+(R)$ in the process of collisional ionization. At a distance R_I the electron leaves the scene with energy $E_{el} = [E^* + V^*(R_I)] - [E^+ + V^+(R_I)]$, without changing the local kinetic energy $E - V^*(R_I) = E' - V^+(R_I)$ of the colliding atoms in the initial and final state, respectively. Both the PI and AI processes of ionization are indicated, together with the initial-state asymptotic energy E and the final-state asymptotic energy E' (PI process) or vibrational quantum number v' (AI process).

Semiclassically, the autoionization width can be interpreted as a decay rate $\Gamma(R)/\hbar$ for the transition to the ionic final state. The largest probability to ionize is at the classical turning point of the initial state potential, where the atoms spend most of their time. This results in a rather peaked yield of ions in this range of R values. When ionization occurs, the electron leaves the scene instantaneously, compared to the heavy particle motion. The kinetic energy of the two colliding particles is conserved, if we neglect the recoil kick by the electron. At low collision energies, the local kinetic energy of the initial state atoms is fully determined by the local depth of the potential, with the well depth as an upper limit. Depending on the details of the initial and final state potentials, the final state products will end up as a molecular ion Ne_2^+ or two free particles Ne^+ and $Ne(^1S_0)$. At low collision energies, the branching ratio for associative ionization is usually in the range of 0.01 to 0.1, fully determined by the details of the initial and final state potentials.

A. Penning ionization

The major part of the ionizing collisions will result in the first reaction path of Eq. (2), with the release of an ion and a ground-state atom with thermal energies. The maximum available kinetic energy now is equal to the well depth of the initial state potential, which is on the order of 250 K. This value is a suitable estimate for the total kinetic energy of the products, equally divided into a kinetic energy $E_{PI} = 125$ K for each of the two heavy particles with equal mass m. The recoil of the electron can be neglected in this case. Secondary collisions of these room-temperature ions and ground state atoms can result in trapped metastable neon atoms being accelerated to thermal velocities, i.e., a finite probabilty for the extra loss of trapped atoms. Grazing collisions can result in heating of the sample of trapped atoms. Both effects are discussed in Sec. IV.

B. Associative ionization

In the center-of-mass system, all energy gained in the potential well of the initial state is stored in the internal degrees of freedom of the final-state dimer ion. In the laboratory system, the dimer ion has an average kinetic energy equal to half the thermal energy of the trapped atoms, as determined by the velocity of the center-of-mass system. This would imply that the dimer-ions, that are in a $^2P_{1/2}$ or in a $^2P_{3/2}$ state with an associated magnetic moment $\mu = \frac{1}{3}\mu_B$ and $2\mu_B$, respectively, would still be trapped in the magnetic trap.

However, in this case, the recoil of the electron has to be taken into account. The increase in energy related to the recoil is

$$E_{AI} = (m_e/m)E_e, \tag{5}$$

with m_e and E_e the electron mass and kinetic energy, respectively. Inserting $E_e = 12$ eV we find $E_{AI} = 1.96$ K corresponding to $\Delta v = 40$ m/s. It is clear that the dimer-ion is not trapped, because the depth of the magnetic trap is much smaller. However, secondary collisions of the hot dimer-ion can result in a small additional loss of trapped atoms per ionization event. Also, grazing collisions can heat up the trapped atoms. These effects are discussed in Sec. IV. Because the cross sections for vibrational and rotational relaxation of the molecular ion are very small, of the order of $10a_0^2$ and less, no internal energy of the dimer ions will be dissipated in the sample of trapped atoms.

IV. HEATING RATE OF TRAPPED ATOMS

Ionizing collisions of the metastable rare gas atoms directly result in the loss of trapped atoms. As shown in Sec. III, the final state products will have large kinetic energies, due to the conversion of potential energy at short range—in the well region—into radial motion. This gives rise to a secondary effect on the trapped atoms: the hot products can collide with a cold trapped atom due to their finite mean free path in the trap. The effect of these secondary collisions is twofold: extra loss and heating.

All large-angle collisions will result in a transfer of energy that is larger than the trap depth $\mathcal{E}$. This results in an extra loss fraction ϵ of trapped atoms, as given by

$$\dot{N}_{loss} = \dot{N}_i(1 + \epsilon),$$

$$\epsilon = \langle l \rangle / \lambda_{sec} = n\langle l \rangle Q_{sec}, \tag{6}$$

with $\dot{N}_i$ the production rate of hot products; λ_{sec} and Q_{sec} are the mean free path and the total cross section for secondary elastic collisions of these hot products with cold trapped atoms, respectively. The distance that a fast particle travels in the trap, averaged over all spatial directions, is indicated by $\langle l \rangle \approx (\pi D/2)$ with D the diameter of the sample. To obtain insight we can insert typical values $Q_{sec} = 10^3 a_0^2$ and $5 \times 10^4 a_0^2$ for atom–metastable-atom and ion–metastable-atom collisions (Sec. V), respectively. For the two final state geometries of the sample in the magnetic trap, we then find
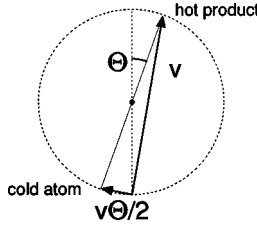
FIG. 5. Newton diagram of the secondary collision of a hot product, atom or ion, with velocity v with a cold trapped atom, showing the corresponding velocity transfer $v\theta/2$ for reduced mass $\mu = m/2$.

$\lambda_{\text{sec}} \geqslant 70$ μm, $\epsilon \leqslant 0.14$ and $\lambda_{sec} \geqslant 360$ μm, $\epsilon \leqslant 0.008$, respectively. The additional loss fraction is thus fully determined by the secondary ion-atom collisions. Clearly, however, the extra loss fraction ϵ is only a minor effect and can be neglected in first order.

But we also have to consider small angle scattering of the hot products with the cold trapped atoms, with a transfer of kinetic energy that is *less* than the trap depth $\mathcal{E}$, which is generally on the order of 10 to 30 mK. However, these small angle collisions will result in trapped atoms with an energy much *larger* than the trap temperature T, which is in the millikelvin to microkelvin range. All of this energy will finally be dissipated in the population of trapped atoms, resulting in an effective heating rate. For a collision of a hot particle (atom, ion, or dimer ion) with velocity v and kinetic energy $E = mv^2/2$ on a stationary target atom, the velocity transfer to the cold atom is given by $\Delta v = v\theta(\mu/m)$, with $\mu = m/2$ and $\mu = 2m/3$ for the hot atoms, atomic ions, and dimer ions, respectively (Fig. 5).

The finite depth $\mathcal{E}$ of the trap results in an upper bound for the energy transfer that will still result in heating but not in the loss of an atom, as determined by $\frac{1}{2}m(\Delta v)^2 \leqslant \mathcal{E}$. This in turn limits the range of scattering angles that we have to take into account

$$\theta \leqslant (m/\mu)(\mathcal{E}/E)^{1/2} = \theta_{\max}. \qquad (7)$$

For collisions with thermal neon atoms at an energy $E_{\text{PI}} = 125$ K in the laboratory system and a trap depth of 50 Gauss (corresponding to $\mathcal{E} = 10$ mK), the maximum scattering angle is $\theta_{\max} = 18$ mrad. This determines the angular range where we need a correct description of the differential cross section $\sigma_{\text{sec}}(\theta)$. In the Sec. IV A we will investigate semiclassical scattering theory, that provides an excellent analytical framework for describing small-angle scattering in thermal collisions [27–30]. In Secs. IV B and IV C we apply these results to obtain an accurate description of the heating rates for atom–metastable-atom and (dimer) ion–metastable-atom secondary collisions.

A. Small-angle differential cross section

In semiclassical theory [27–31], the small-angle differential cross section $\sigma_{\text{sec}}(\theta)$ scales with the characteristic diffraction angle

$$\theta_{0,\text{sec}} = (4\pi/k^2 Q_{\text{sec}})^{1/2}, \qquad (8)$$

with $k = \mu v/\hbar$ the wave number and v the relative velocity of the collision partners. For an inverse power-law potential $V(R) = C_s/R^s$ (with $s = 4$ for the charge-induced dipole interaction of ion-atom scattering, $s = 6$ for the induced dipole-dipole nature of atom-atom scattering), simple analytical formulas are available.

For angles $\theta \ll \theta_{0,\text{sec}}$ we observe a *diffraction* peak, which can be approximated by [31,32]

$$\sigma_{\text{sec}}(\theta)/\sigma_{\text{sec}}(0) = 1 - \alpha_1(s)(\theta/\theta_{0,\text{sec}})^2, \qquad (9)$$

with $\alpha_1(s)$ a numerical constant given in Table II. For angles $\theta \gg \theta_{0,\text{sec}}$ we find the classical result [29–31]

$$\sigma_{\text{sec}}(\theta)/\sigma_{\text{sec}}(0) = \alpha_2(s)(\theta/\theta_{0,\text{sec}})^{-2(s+1)/s}, \qquad (10)$$

which corresponds to *refraction*, in analogy to geometrical optics when scattering light on an inhomogeneous medium. The constant $\alpha_2(s)$ is given in Table II. Successful semiempirical formulas connecting the two regions are given by several authors [29,31]. The absolute value of the differential cross section $\sigma_{\text{sec}}(0)$ in the forward direction and the total elastic cross section Q_{sec} are given by [33,34]

$$\sigma_{\text{sec}}(0) = k^2 Q_{\text{sec}}^2/\{16\pi^2 \cos^2[\pi/(s-1)]\},$$

$$Q_{\text{sec}} = \alpha_3(s)(C_s/\hbar v)^{2/(s-1)}, \qquad (11)$$

with $\alpha_3(s)$ given in Table II. To obtain insight in the fraction of the total cross section in the forward diffraction peak for $\theta \leqslant \theta_{0,\text{sec}}$ and the refraction dominated range for $\theta \gg \theta_{0,\text{sec}}$, we can calculate the integral of these approximations of the differential cross section in these intervals. We find that 15 to 25 % of the cross section is in the diffraction peak (depending on the value of s), with the remainder in the refraction dominated region.

Typical values of the cross sections are given in Table II for both $\text{Ne}(^1\text{S}_0) + \text{Ne}^*$ and $\text{Ne}^+ + \text{Ne}^*$ secondary collisions at an energy $E_{\text{PI}} = 125$ K, as relevant for the PI process. For the AI process typical values of the cross sections are given for $\text{Ne}_2^+ + \text{Ne}^*$ secondary collisions at an energy $E_{\text{AI}} = 2$ K, as determined by the recoil of the electron.

The lower limit on the energy where this semiclassical description starts to fail is determined by the condition that sufficient partial waves contribute to the scattering cross sections. For the neon system p waves start to contribute at 10 mK [6]. This implies that the lower limit for our model for heat transfer is still valid at 2K, the energy release in associative ionization. We can now identify which models we have to apply to calculate the heating rates for the case of atom–metastable-atom scattering and (dimer) ion–metastable-atom scattering, by comparing the maximum scattering angle to the scaling angle.

1. Atom–metastable-atom scattering: s = 6

For thermal collisions of neon atoms in the ground state with trapped metastable atoms the collision process is dominated by the induced dipole-dipole interaction, characterized by the long range C_6/R^6 potential. In this case, the maximum scattering angle $\theta_{\max}$ is always much *smaller* than the

TABLE II. Parameters for secondary collisions of hot, final state products of residual ionizing $Ne|2,2\rangle$ $+ Ne|2,2\rangle$ collisions with cold trapped atoms, assuming a kinetic energy $E_{PI} = 125$ K and $E_{AI} = 2$ K for the hot product from the PI and the AI process, respectively. The resulting heating rate $\dot{T}_{sec}$ of the total population of trapped atoms is given for both the high-density–low-aspect-ratio and low-density–high-aspect-ratio case of the final state. The depth of the magnetic trap is fixed to $\mathcal{E} = 10$ mK.

	$Ne(^1S_0) + Ne^*$ PI, $E_{PI} = 125$ K	$Ne^+ + Ne^*$ PI, $E_{PI} = 125$ K	$Ne_2^+ + Ne^*$ AI, $E_{AI} = 2$ K
s	6	4	4
$\alpha_1(s)$	0.9975		
$\alpha_2(s)$	0.2846	0.1920	0.1920
$\alpha_3(s)$	8.083	11.37	11.37
C_s (a.u.) [a]	52.7	103.9	103.9
μ (a.u.)	10	10	13.33
v (m/s)	322	322	57
k (a_0^{-1})	2.7	2.7	0.63
Q_{sec} (a_0^2)	1.35×10^3	9.03×10^4	2.88×10^5
$\sigma_{sec}(0)(a_0^2)$	1.28×10^5	1.50×10^9	8.36×10^8
$\theta_{0,sec}$ (mrad)	36	4.4	10.5
$\theta_{max}/\theta_{0,sec}$	0.50	4.1	7.3
$\Delta Q_{sec}/Q_{sec}$	0.095		
$\Delta E(\theta_0)$(mK)		0.60	0.2
$\dot{T}_{sec}$ (μK/s) [b]	$0.60 \times \eta_{PI}$	$104 \times \eta_{PI}$	$249 \times \eta_{AI}$
$\dot{T}_{sec}$ (μK/s) [c]	$0.007 \times \eta_{PI}$	$1.25 \times \eta_{PI}$	$3.0 \times \eta_{AI}$

[a]References [36] and [35].
[b]High density case with $T_C = 1.7$ μK (Table I).
[c]Low density case with $T_C = 0.6$ μK (Table I).

characteristic angle $\theta_{0,sec}$ (Table II and Fig. 6). This statement holds for a wide range of collision energies, due to the scaling law $\theta_{max}/\theta_{0,sec} \sim E^{-1/[2(s-1)]} = E^{-1/10}$ that can easily be derived using Eqs. (8) and (11). Therefore the *diffraction region* in the differential cross section [Eq. (9)] will be most
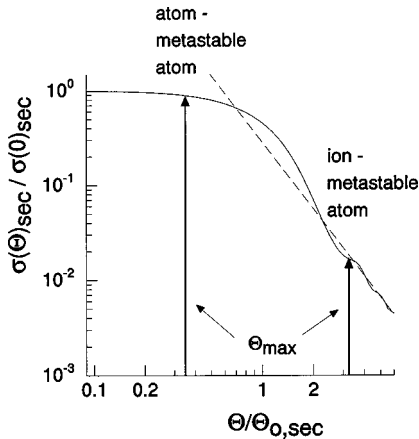

FIG. 6. Small-angle differential cross section $\sigma_{sec}(\theta)/\sigma_{sec}(0)$ for the case of a C_6/R^6 potential for atom–metastable-atom thermal collisions. Full line: quantum-mechanical calculations; dashed line: classical mechanics. The results are also indicative for scattering on a C_4/R^4 potential for ion–metastable-atom collisions. Typical values for the maximum scattering angle θ_{max} are indicated for the case of atom–metastable-atom and ion–metastable-atom secondary collisions, respectively.

important for calculating the heating rate for atom–metastable-atom collisions.

2. Ion−metastable-atom scattering: $s = 4$

For thermal collisions of neon ions and dimer ions with the trapped metastable atoms the interaction is determined by the charge-induced dipole interaction, characterized by a long range C_4/R^4 potential that extends to larger internuclear seperations R. In this case, the total cross section is much larger than for the thermal collisons with the ground-state atoms, resulting in a much smaller value of the characteristic angle $\theta_{0,sec}$. In this case, the maximum scattering angle is always much *larger* than the characteristic angle. The *refractive region* of the differential cross section [Eq. (10)] will give the largest contribution to the heating rate.

B. Heating by atom−metastable-atom collisions

Using Eqs. (8), (9), and (11) we can now calculate the heat transfer rates for atom–metastable-atom collision processes by inserting $s = 6$. The effective total cross section ΔQ_{sec} for the transfer of heat can be approximated by

$$\Delta Q_{sec} \approx (\pi \theta_{max}^2) \sigma_{sec}(0), \qquad (12)$$

using a constant value for the forward differential cross section. The rate of increase of the total energy U, i.e., kinetic energy plus potential energy, of the trapped atoms is then given by

$$\dot{U} = (n\langle l\rangle \Delta Q_{\text{sec}})(\Delta E)\dot{N}_i, \qquad (13)$$

with $(n\langle l\rangle \Delta Q_{\text{sec}})$ the probality ''density $\times$ length $\times$ cross section'' for a grazing collision and $\dot{N}_i$ the production rate of hot atoms or ions, i.e., the ionization rate. The average amount of transferred kinetic energy, given by $\Delta E = \mathcal{E}/2$, is calculated by integrating $\frac{1}{2}m(\Delta v)^2$ over the angular range between 0 and θ_{max}. We assume N trapped atoms in a harmonic potential with six degrees of freedom, with a total energy $U = N(3k_B T)$. The heating rate $\dot{T}$ of the trapped atoms is then given by

$$\dot{T} = (n\langle l\rangle \Delta Q_{\text{sec}})(\mathcal{E}/6k_B)/\tau_i. \qquad (14)$$

Equation (13) was simplified by the substitution $\dot{N}_i/N = 1/\tau_i$, with τ_i the time constant for ionization.

Insight is obtained when we investigate the scaling of Eq. (12) with the parameters related to the trapped species and the inelastic collisions leading to the trap loss, resulting in

$$\Delta Q_{\text{sec}} \sim \mathcal{E}(\mu^{7/5} C_4^{4/5} E^{-2/5}). \qquad (15)$$

The dependency on both C_4 and E can be easily understood. With decreasing energy E, the mean free path for small angle scattering decreases. This is due to the increase $Q_{\text{sec}} \sim C_s^{2/5} E^{-1/5}$ of the total cross section for secondary collisions and the corresponding increase $\sigma_{\text{sec}}(0) \sim Q_{\text{sec}}^2$ of the differential cross section. Inelastic collisions with a *small* release of energy thus result in a *larger* dissipation of energy in the sample of trapped atoms, a rather counterintuitive result.

A last remark concerns the dependency of the heating rate on the trap depth, as given by $\dot{T} \sim \mathcal{E}^2$. A smaller value of $\mathcal{E}$ results in both a smaller average value of the transfered energy [Eq. (14)] as well as a smaller range of forward scattering that contributes [Eqs. (7) and (12)]. Choosing for an experimental setup with a small value of $\mathcal{E}$ is thus advantageous for lowering the heating rate.

C. Heating by (dimer) ion–metastable-atom collisions

For the calculation of the heating rate for (dimer) ion–metastable-atom collisions we use Eqs. (8), (10), and (11) for $s = 4$. The effective product $\Delta(QE)$ of the partial cross section and the energy transfer is given by the integral

$$\Delta(QE) = \int_0^{\theta_{\text{max}}} \sigma_{\text{sec}}(\theta)\Delta E(\theta) 2\pi\theta d\theta = [4\alpha_2(s)/3]$$
$$\times(\pi\theta_{0,\text{sec}}^2)\sigma_{\text{sec}}(0)\Delta E(\theta_{0,\text{sec}})(\theta_{\text{max}}/\theta_{0,\text{sec}})^{3/2}, \qquad (16)$$

with $\Delta E(\theta) = (m/2)(v\theta\mu/m)^2$ the energy transfer corresponding to a scattering angle θ. By using the accidental relationship $(\pi\theta_{0,\text{sec}}^2)\sigma_{\text{sec}}(0) = Q_{\text{sec}}$ for a potential with $s = 4$ and the substitution $\theta_{\text{max}}/\theta_{0,\text{sec}} = [\mathcal{E}/\Delta E(\theta_{0,\text{sec}})]^{1/2}$ we obtain

$$\Delta(QE) = 0.25 Q_{\text{sec}}\Delta E(\theta_{0,\text{sec}})^{1/4}\mathcal{E}^{3/4}. \qquad (17)$$

The heating rate of the trapped atoms in a harmonic potential then is equal to

$$\dot{U} = (3k_B\dot{T})N = n\langle l\rangle \Delta(QE)\dot{N}_i,$$
$$\dot{T} = 0.25(n\langle l\rangle Q_{\text{sec}})[\mathcal{E}^{3/4}\Delta E(\theta_{0,\text{sec}})^{1/4}/3k_B]/\tau_i. \qquad (18)$$

Compared to the expression for the heating rate for atom–metastable-atom collisions in Eq. (14), the major difference is the occurrence of the full value of the total cross Q_{sec} in the collision probability ''density $\times$ length $\times$ cross section'' in Eq. (18) as compared to the much smaller fractional cross section ΔQ_{sec} in Eq. (14). This results in a scaling $\dot{T} \sim \mathcal{E}^{3/4}$ of the ion–metastable-atom heating rate with the trap depth $\mathcal{E}$: lowering the trap depth thus results in a much slower decrease of the heating rate than is the case for atom–metastable-atom collisions.

The implications for the heating rate by dimer ion–metastable-atom collisions are even more severe. Due to the very small collison energies of the dimer ions (resulting from the recoil kick of the electron in the AI process) and the scaling $Q_{\text{sec}} \sim E^{-1/4}$, we expect a large cross section and thus a large heating rate for these collisions. However, a small value of the branching ratio η_{AI} to the process of Associative Ionization will most likely limit the effect on the heating rate.

D. Heating by UV-photon recoil

Finally, we also have to consider the heating effect by the recoil kick of the UV photon emitted in the radiative decay of the metastable atom. This kick corresponds to an energy ΔE_{uv} in the 50 μK to 1 mK range. At these collision energies only s waves contribute to the scattering process, with a cross section fully determined by the scattering length. However, in this case it concerns the scattering length $a_{0,2}$ for collisions of atoms in the ground state with the trapped metastable atoms. The effective heating rate is then given by

$$\dot{U} = (n\langle l\rangle Q_{T=0})(E_{\text{uv}})\dot{N}_{\text{uv}},$$
$$\dot{T} = (n\langle l\rangle Q_{T=0})(E_{\text{uv}}/3k_B)/\tau_{\text{uv}} \leq (E_{\text{uv}}/3k_B)/\tau_{\text{uv}}, \qquad (19)$$

with $Q_{T=0} = 8\pi a_{0,2}^2$ the s-wave scattering cross section. To obtain the second equation we have substituted $\dot{N}_{\text{uv}}/N = 1/\tau_{\text{uv}}$. Again we have assumed a harmonic trap with six degrees of freedom. Compared to the results for atom–metastable-atom and ion–metastable-atom scattering, the finite depth of the trap plays no role because $E_{\text{uv}} \ll \mathcal{E}$. The heating rate only depends on the finite radial dimension $\langle l\rangle$ of the trap. The upper limit corresponds to the case of an infinite scattering length $a_{0,2} \to \infty$, when the total recoil energy is dissipated in the sample.

V. HEATING RATES FOR NEON

In Table II we have listed the collision parameters that serve as input for the calculation of the heating rate for neon. The C_4 [35] and C_6 [36] values originate from theory, but

TABLE III. Heating lifetime $\tau_{\text{heat}} = T_C / \dot{T}_{\text{sec}}$ of the total population of trapped atoms by secondary collisions of hot, final-state products of residual ionizing collisions with cold trapped atoms at the onset of condensation at temperature T_C. In these calculations we have assumed continuous evaporative cooling with a cutoff at an energy $\mathcal{E} = 6 k_B T_C$. The results are given for neon and helium, using the input data of Tables II and V. Both the high-density–low-aspect ratio and the low-density–high-aspect ratio of the condensate state are investigated.

	Ne		He	
	High density	Low density	High density	Low density
$R(^1S_0) + R^*$	$2.7 \times 10^6 / \eta_{\text{PI}}$	$6.6 \times 10^8 / \eta_{\text{PI}}$	$1.8 \times 10^7 / \eta_{\text{PI}}$	$3.8 \times 10^9 / \eta_{\text{PI}}$
$R^+ + R^*$	$2.9 / \eta_{\text{PI}}$	$183 / \eta_{\text{PI}}$	$4.9 / \eta_{\text{PI}}$	$313 / \eta_{\text{PI}}$
$R_2^+ + R^*$	$1.2 / \eta_{\text{AI}}$	$77 / \eta_{\text{AI}}$	$2.5 / \eta_{\text{AI}}$	$159 / \eta_{\text{AI}}$

are expected to be close (within 10%) to reality considering the current status of this type of calculations. For the energy of the ion and atom released in the process of Penning ionization we have used $E_{PI} = 125$ K, as discussed in Sec. III. The scaling law $\dot{T} \sim E^{-2/(s-1)}$ can always be applied to obtain the heating rate at other values of the energy release. For the process of associative ionization we haved used the recoil energy of the electron as the collision energy (Sec. III). The C_4 value for the $Ne_2^+ + Ne^*$ system has been fixed at the value for the $Ne^+ + Ne^*$ system. The depth of the trap has been fixed to $\mathcal{E} = 10$ mK, resulting in a maximum scattering angle $\theta_{\text{max}} = 18$ mrad for atom–metastable-atom and ion–metastable-atom scattering and $\theta_{\text{max}} = 76$ mrad for the low energy dimer ion–metastable-atom collisions.

To compare the contributions from the PI and the AI process we assume a branching ratio $\eta_{\text{AI}} = 0.1$. We observe that ion–metastable-atom collisions, resulting from the long-range ion-induced dipole interaction, are the dominant contribution to the heating rate. Due to the small branching ratio, the even larger heat transfer *per collision* for the dimer ion results in a smaller contribution to the heating rate.

For the scaling of the heating rate with respect to the number density and the geometry of the sample of trapped atoms we find

$$\dot{T} \sim n^2 \langle l \rangle, \tag{20}$$

which is obtained by substituting $\tau_i = 1/(\mathcal{K}_i^{\text{pol}} n)$ in Eq. (18). To decrease the heating rate without affecting the conditions where BEC occurs, we have to choose for a tighter confinement in the radial direction. By lowering the number density n we also lower the value of the transition temperature T_C according to Eq. (1). The heating lifetime τ_{heat} at the transition temperature T_C then scales as

$$\tau_{\text{heat}} = T_C / \dot{T} \sim n^{-4/3}, \tag{21}$$

which helps us to choose favorable geometries for obtaining BEC.

The heating rates have been calculated for both final state trap geometries. For the value of $\langle l \rangle$ we use the radial size given in Table I. For the high-density–low-aspect-ratio case the total heating rate of 119 μK/s is fatal for achieving BEC at the transition temperature $T_C = 1.7 \mu$K. For the low-density–high-aspect-ratio case the total heating rate of

1.4 μK/s compares favorable to the value $T_C = 0.6 \mu$K, resulting in a heating lifetime of approximately 0.5 s. This value has to be compared to the lifetime $\tau_i = 5$ s for ionization.

Finally, we have also investigated the heating rate at the BEC transition temperature, where we assume that the process of evaporative cooling is left switched on with a cutoff at $6 k_B T_C$. This results in an effective trap depth $\mathcal{E}$ equal to this cutoff value, which limits the scattering angle θ_{max} to values much smaller than $\theta_{0,\text{sec}}$ with a correspondingly smaller heating rate for the ion–metastable-atom collisions. In Table III we show the heating lifetime τ_{heat} [Eq. (21)] for the final state at the transition temperature T_C. Typical lifetimes τ_{heat} are then always much larger than the lifetime for ionization, both for the high-density and the low-density case. Keeping the process of evaporative cooling switched on in the final state at the transition temperature is thus very effective: the heating rate is lowered by two orders of magnitude while we also profit from the ongoing cooling effect. The latter has not been taken into account in this calculation.

The decay of the metastable state with a lifetime $\tau_{\text{uv}} = 24$ s results in the emission of a UV photon with a wavelength of 70 nm, with an associated recoil kick of the atom equal to 25 cm/s corresponding to an energy $E_{\text{uv}} = 60 \mu$K. No information at all is available on the actual value of the scattering length $a_{0,2}$ for cold atom–metastable-atom collisions, which is required for evaluating Eq. (19). If we assume a scattering length $a_{0,2} = 100 a_0$, we find a mean free path $(n Q_{T=0})^{-1} = 14$ and 71 μm for the high-density–low-aspect-ratio and the low-density–high-aspect-ratio cases, respectively. The resulting heating rates are given in Table IV. For this large value $a_{0,2} = 100 a_0$ of the scattering length, the heating rate is always less than the heating rate for ion–metastable-atom collisions. This even holds for the case of an infinite scattering length $a_{0,2}$.

We conclude that the low-density–high-aspect-ratio final state is the best choice for achieving BEC. Keeping the process of evaporative cooling switched on at T_C extends the heating lifetime to values larger than the ionization lifetime of 5 s.

VI. TRAPPING AND COOLING FEATURES

A. Bright atomic beam

For loading the trap, an atomic beam of cold atoms is the only choice [37–42]. In Eindhoven, a bright beam line is

TABLE IV. Heating rate $\dot{T}$ of the trapped population for the high-density–low-aspect-ratio and low-density–high-aspect-ratio configurations of the final state, respectively, by the recoil of the UV photon emitted during the radiative decay of the metastable atom. Data are given both for neon and helium, as a function of the scattering length $a_{0,2}$ for atom–metastable-atom cold collisions.

| | | Ne | | He | |
		High density	Low density	High density	Low density
$a_{0,2}=50a_0$	$\dot{T}$ (μK/s)	0.14	0.009	0.007	0.0005
$a_{0,2}=100a_0$	$\dot{T}$ (μK/s)	0.57	0.035	0.029	0.002
$a_{0,2}\rightarrow\infty$	$\dot{T}$ (μK/s)	0.83	0.83	0.041	0.041

available for this purpose, routinely delivering a total flux of 5×10^{10} metastable neon atoms per second in the $^3P_2$ state [39]. The beam characteristics are an axial velocity of 100 m/s in a 1 mm diameter beam with a divergence of 3 mrad, designed for applications in intrabeam scattering experiments. By combining a beam stop in the upstream part with a beam-limiting collimator in the downstream end beyond the beam compressor, the atomic beam only consists of cold $^{20}Ne(^3P_2)$ metastable atoms. All undesired beam components are removed, such as thermal energy neon atoms in the ground state, thermal $Ne(^3P_0)$ and $^{22}Ne(^3P_2)$ metastable atoms, and UV photons from the discharge-excited atomic beam source.

A variety of laser cooling techniques is used in this beam line. The atoms leaving a LN_2-cooled discharge-excited beam source are captured in a collimator with a 100 mrad acceptance; after an extra transverse Doppler-cooling stage, the atoms enter a midfield-zero Zeeman slower. Then, a magneto-optical compressor tightens the beam to its desired diameter, with a sub-Doppler transverse cooling stage to mold it into the desired beam divergence. A single cw dye laser is used for operating the beam line, using AOM's to shift the laser frequency for the different stages of laser cooling.

B. MOT

To be trapped in a magneto-optical trap (MOT), the beam of cold atoms has to be decelerated from its original velocity of 100 m/s to a velocity less than 15 m/s. The stopping distance is on the order of 10 mm, leaving a variety of methods to achieve this. First, the MOT laser beams, crossing the atomic beam at a 45 ° angle and red detuned by a few linewidths, are nearly sufficient to slow the atoms to the trapping velocity. Also, an extra laser beam can be employed, with a free choice of angle and detuning. For the MOT, we opt for a low density and a large diameter, to avoid large trap losses due to ionization of the unpolarized population. Typically, we can load $N\geq10^{10}$ atoms in the MOT with a loading time of 1 s. As a radius we choose $r=5$ mm, resulting in an equilibrium density of 1.9×10^{10} cm^{-3} with a corresponding decay time for ionization equal to $\tau_i=0.7$ s. For the temperature in the MOT we expect a value of the order of $T\approx100$ μK.

C. Magnetic trap

Finally, the population has to be transferred from the MOT to a magnetic trap. The $Ne(^3P_2)$ state has a Landé

factor $g_J=1.5$, leading to a dipole moment of $3\mu_B$ with a potential energy of 0.202 mK per Gauss. For a three-dimensional harmonic trap the BEC condition of Eq. (1) can be written as [43]

$$k_BT_C=0.94\hbar\bar{\omega}N^{1/3}, \qquad (22)$$

with $\bar{\omega}=(\omega_r^2\omega_z)^{1/3}$ the geometric mean value of the frequencies of the confining potential. For the high-density–low-aspect-ratio and the low-density–high-aspect-ratio cases we find $\bar{\omega}=382$ (2π) Hz and 224 (2π) Hz, respectively. To satisfy our demands on the tight radial confinement, with a typical radial dimension of 10 and 3 μm, we find radial frequencies equal to $\omega_r=500$ (2π) Hz and $\omega_r=1000$ (2π) Hz for the high- and the low-density cases, respectively. The corresponding axial frequencies and aspect ratios A then are $\omega_z=222$ (2π) Hz, $A=2.2$, and $\omega_z=12$ (2π) Hz, $A=83$.

Both a Ioffe-Pritchard trap [44] or a clover-leaf trap [19] can be used for a trap with a tight radial confinement and a large aspect ratio, the latter choice being required to obtain a sufficiently large population N of trapped atoms. Using a clover-leaf coil configuration, a radial frequency $\omega_r=1000$ (2π) Hz can be achieved with a radial gradient $B_r'=150$ G/cm and a bias field $B_0=0.5$ G. The former gradient can be readily achieved in a clover-leaf coil configuration with a 100 mm distance between the two planes where the coils are located, leaving sufficient space for a trapping chamber and diagnostics.

To match the size of the magnetic trap to the MOT, it is required to widen up the trap by increasing the bias field B_0, thus decreasing the radial frequency and increasing the radial dimensions to a few mm. We assume that 10^{10} atoms in the $|2,2\rangle$ state are loaded in the trap. Next, we apply an adiabatic compression by a decrease of the bias field, with a decrease in volume and a corresponding increase in temperature. At the onset of evaporative cooling, we assume a temperature $T=2$ mK and a density of $n=5\times10^{11}$ cm^{-3} with an associated trap lifetime for residual ionization of $\tau_i=200$ s.

D. Evaporative cooling

In this section we use the recent review paper by Ketterle and Van Druten [21] as a starting point. The essential parameter of evaporative cooling is the ratio R of ''good collisions'' to ''bad collisions.'' The larger this number is, the

easier it is to get into the regime of runaway evaporative cooling with an increasing elastic collision rate. As yet, no accurate information at all is available on the potentials for binary collisions of metastable neon atoms. The scattering length $a_{2,2}$, which determines the cross section Q_{el} $=8\pi a_{2,2}^2$ and the rate constant $\mathcal{K}_{el}=\langle v\rangle Q_{el}$ for elastic scattering at these low energies, are thus unknown.

For the alkali gases, collisions with the background gas are the dominant factor for the loss of atoms from a magnetic trap. For the metastable rare gases the situation is different. At a background pressure of 10^{-9} Torr, the trapping time due to these collisions is on the order 20 s, using a typical rate constant $\mathcal{K}_{gas}\approx 1.6\times10^{-9}$ cm^3 s^{-1} for collisons with the background gas. In the initial state of the trapped metastable neon atoms, with $\tau_i=200$ s, the collisions with the background gas determine the trapping time. This situation is identical to the alkali gases. For the two final state geometries of Table I, the lifetime τ_i for ionization is at least a factor four smaller than the trapping time for background collisions.

In the final state, the residual ionizing collisions of the polarized metastable neon atoms are the dominant contribution to the ''bad collisions.'' This is identical to the case of H atoms, where spin-changing binary collisions are the major loss process [20]. The elastic collision rate $n\mathcal{K}_{el}$ as well as the rate of suppressed ionization $n\mathcal{K}_i^{pol}$ then have the same dependency on the density n in the trap: the ratio R of ''good collisons'' to ''bad collisions'' is independent of density and scales as $T^{1/2}$.

For the case of metastable neon, the evaporative cooling thus evolves from an ''alkalilike'' initial state to a ''hydrogenlike'' final state. For the initial and final state the ratio R is given by

$$R=n\mathcal{K}_{el}/n_{gas}\mathcal{K}_{gas}, \quad \text{initial state,}$$

$$R=\mathcal{K}_{el}/\mathcal{K}_i^{pol}\geq\langle v\rangle 8\pi a_{2,2}^2/(\mathcal{K}_i^{pol})_{max}=R_{min}, \quad \text{final state,} \tag{23}$$

with $\langle v\rangle$ the average velocity of the trapped atoms and $(\mathcal{K}_i^{pol})_{max}$ given in Eq. (4). Numerical values for R_{min} are given in Table I. We have to compare these minimum values to the requirement $R\geq120$ and 450 for run-away cooling in a linear trap (initial state at $T=2$ mK) and a harmonic trap (final state), respectively. For the initial state, it is very easy to achieve conditions of runaway cooling. Depending on the actual value of the scattering length $a_{2,2}$, the cooling can slow down when getting closer to the final state. In the case of scattering length $a_{2,2}\geq50a_0$ the conditions of runaway cooling are fulfilled in the whole cooling range from 2 mK to 1 μK.

To estimate the time required for the phase of evaporative cooling, we use the results of Van Druten and Ketterle. For the case of a harmonic potential and a cutoff at an energy equal to $6k_bT$, we find an increase of phase space density by a factor 10^6 in 600 elastic collision times with a loss in total population by a factor 100. Lowering the cutoff to, e.g., a value of $5k_BT$ gives the same increase in phase-space density in half the number of collisions, at the price of ending up

with five times fewer atoms. For the case of metastable neon we find an elastic collision rate of 113 s^{-1} for the initial state; for the final state we find 665 and 78 s^{-1} for the high-density and the low-density case, respectively, when assuming a scattering length equal to $a_{2,2}=50a_0$. Cooling times of a few seconds can be achieved in this case, especially if we keep in mind that we have assumed a loss in population by a factor 10^4 throughout this paper. This opens the possibility of applying rather low values of the cutoff, resulting in cooling times that are always much less than the ionization time. This always holds for the initial state with $\tau_i=200$ s; only a small fraction of the cooling time is most likely spent close to the final state densities with $\tau_i=1$ and 5 s, respectively.

Because ionization is a two-body collision process, the loss of metastable atoms will preferentially occur on the z axis of the magnetic trap where the density is high. These atoms have a lower than average potential energy: their loss will thus result in an effective heating of the remaining population of trapped atoms. If we assume an average potential energy of $k_BT/2$ of these centerline atoms, the effective energy transfer is equal to the remaining fraction k_BT of potential energy. We can directly derive a heating rate equal to $\dot{T}=(2T/3)/\tau_i$. For the final state geometries investigated, this results for neon in $\dot{T}=1.1$ μK/s and $\dot{T}=0.08$ μK/s for the high density and low density case, respectively. These rates are independent of the depth of the trap. Keeping the evaporative cooling switched on after having reached BEC is the solution for this problem.

E. Mimimizing the trap depth

Looking at the scaling of the heating rates with the trap depth, we conclude that it is important to choose for the lowest value of $\mathcal{E}$ that can be experimentally obtained for metastable atoms escaping in all directions. A simple method is to add an open-ended glass tube with radius r_w, placed on axis with the z axis of the magnetic trap. The inner wall of the tube now acts as a ''wall of death'' for atoms with an energy larger than the magnetic energy $\mu B_r' r_w$: metastable atoms are de-excited by a surface collision. For neon atoms with a magnetic energy of 0.202 mK/G, a trap depth of 10 mK corresponds to a maximum magnetic field $B=50$ G. With a gradient of 100 G/cm this translates to $r_w=5$ mm. Care has to be taken, however, that the MOT laser beams are not disturbed in such a way that insufficient atoms can be loaded. The actual design is clearly a tradeoff between these two demands.

VII. REAL-TIME DIAGNOSTICS

A spin-polarized sample of metastable atoms trapped in a magnetic trap can be monitored by observing the loss processes. First, the finite lifetime of the metastable state ($\tau_{uv}=24$ s for neon) results in a flux of UV photons by the radiative decay to the ground state. The trapped population $N(t)$ decays exponentially according to $N(t)=N(0)\exp(-t/\tau_{uv})$, which can be easily monitored using a channeltron. The count rate S_{uv} for UV-photons is equal to

$$S_{\text{uv}} = \eta_{\text{uv}} \Omega_{\text{uv}} N(t)/\tau_{\text{uv}}, \qquad (24)$$

with η_{uv} the quantum efficiency of the detector and Ω_{uv} the solid angle acceptance. Assuming $\eta_{\text{uv}} = 1$ and $\Omega_{\text{uv}} = 10^{-2}$ sr, the count rate ranges from $S_{\text{uv}} = 2.8 \times 10^5$ s^{-1} in the initial state of the trapped sample to the order of 10 s^{-1} in the final state (Table I). These count rates are quite sufficient to track the evolution of the population during the phase of evaporative cooling.

The residual ionization of the trapped atoms results in ions leaving the sample at a rate S_i of

$$S_i = -\frac{dN}{dt} = (\mathcal{K}_i^{\text{pol}})\frac{n^2}{2} V = (\mathcal{K}_i^{\text{pol}}) nN/2, \qquad (25)$$

with $V = N/n$ the effective volume of the trapped sample. This results in an ion count rate $S_i = 5 \times 10^7$ in the initial state; in the final state we find $S_i = 10^6$ and 4×10^4 s^{-1} for the high density and the low density case, respectively, assuming a quantum efficiency of unity for the detector used. These count rates allow us to measure the evolution of the density of the sample on a time scale of microseconds to milliseconds, an interesting prospect.

Finally, we can also measure the density of the trapped $|2,2\rangle$ atoms by an external probe. A short laser pulse, at a frequency tuned to a transition to a short-lived Ne($3p, |J = 1, m_J = 1\rangle$) state, will result in a small fraction of atoms in the ionizing Ne($3s, {}^3\text{P}_0$) metastable state. The extra yield S_x of ions due to this ionizing fraction is given by

$$S_x = -\frac{dN_x}{dt} = \mathcal{K}_{i,x} n N_x = N_x/\tau_x, \qquad (26)$$

with N_x the total number of atoms in state $|x\rangle$. The decay time $\tau_x = (n\mathcal{K}_{i,x})^{-1}$ of the extra contribution to the ion count rate is a direct measure for the absolute density n of the trapped $|2,2\rangle$ state. The calculated value for $\mathcal{K}_{i,x}$ is the scaling factor relating the time scale to the density scale. For the initial state we find $\tau_x = 25$ ms; for the final state $\tau_x = 125$ and 625 μs for the high and the low density case, respectively. When ionizing a fraction $N_x = 10^{-3}N$ of the total population per probe pulse, the peak count rates S_x for the initial and final state are always larger than the steady-state ion signal S_i (Table I). In all cases we find $S_x/S_i \gtrsim 8$, which is a sufficient signal-to-background ratio for an accurate measurement of the decay time.

Using Eqs. (24), (25), and (26) we have three linear equations with two parameters, i.e., the density n and the population N of the trapped $|2,2\rangle$ atoms. The ionization rate constant $\mathcal{K}_{i,x}$ can be determined reliably from intra-beam collision experiments with cold atoms, with an estimated accuracy of 20 to 30 %. At the initial state conditions, with fairly high count rates for all three diagnostics, we can then determine the rate constant $\mathcal{K}_i^{\text{pol}}$ for the residual ionization. When this calibration has been done, we can limit ourselves to the two non-invasive measurements of S_{uv} and S_i; the probe pulse method is only necessary for small sample sizes, where the UV count rate gets too low for accurate data on N in a short time step.

The measured values for n and N can be combined with the field geometry of the magnetic trap to reveal the temperature T of the trapped atoms. At high temperatures, as encountered in the initial stage at the onset of evaporative cooling, the trap is linear in the radial direction and harmonic in the axial direction. At low temperatures the trap is harmonic in all three dimensions. This results in

$$N/n \sim V \approx \frac{(2k_B T/m)^{1/2}}{\omega_z} \left(\frac{k_B T}{3\mu_B B'_r}\right)^2 \sim T^{5/2}, \quad \text{high } T,$$

$$N/n \sim V \approx \prod_{j=1}^{3} \frac{(2k_B T/m)^{1/2}}{\omega_j} \sim T^{3/2}, \quad \text{low } T, \qquad (27)$$

where we have set the temperature equal to the trapping potential to calculate the characteristic size of the sample. We conclude that the density, temperature, and total population of a sample of metastable atoms trapped in a magnetic trap can be monitored in real time using two channeltrons for detecting the ions and the UV photons, respectively.

VIII. COMPARISON TO METASTABLE HELIUM

Currently, the group of Hogervorst in Amsterdam is actively pursuing BEC in metastable helium. [12,13]. At first glance, the triplet metastable He* $(1s)(2s)$ ${}^3\text{S}_1$ atom with its long lifetime of 9000 s [45] and an isotropic electrostatic interaction, seems to be the best candidate for achieving BEC. The first theoretical results for the calculated small rate constant for residual ionization, driven by magnetic dipole-dipole interactions, indicate a suppression of 10^4. However, the large recoil related to its light mass results in drawbacks in laser cooling and trapping of large fluxes of atoms. This implies lower trap densities, smaller values of the transition temperature T_C and correspondingly longer evaporative cooling times. This longer time scale results in a stronger influence of trap losses and associated heating by collisons with the background gas.

However, for our comparison of helium with neon, we assume *equal* loading rates and *equal* densities. This avoids a long discussion on experimental advantages and disadvantages of both systems. At the final density, the lifetime of the trapped helium atoms is equal to the neon results, due to the comparable values of the rate constant for residual ionization. At equal density, the transition temperature scales as $T_C \sim m^{-1}$, resulting in $T_C = 8.6$ μK and 2.9 μK for the high density and low density case, respectively.

In Table V we have listed the parameters used to calculate the heating rate for the trapped metastable helium atoms in the final state. Because the well depth of the initial state is on the order of 1000 K, deeper than is the case for neon, we have used $E_{\text{PI}} = 500$ K for the product energy in the PI process. For the AI process we have used $E = 17$ K as determined by the electron recoil. For helium the branching ratio for ionizing collisions has been determined experimentally by Müller *et al.* and Mastwijk, resulting in $\eta_{\text{AI}} = 0.07$ at $E = 17$ K [9] and $\eta_{\text{AI}} = 0.030$ at 0.1 μK [41], respectively. For the high density case the total heating rate then is

TABLE V. Parameters for secondary collisions of hot, final state products of residual ionizing $He|1,1\rangle$ $+He|1,1\rangle$ collisions with cold trapped atoms, assuming a released kinetic energy per particle of E_{PI} $=500$ K for the PI and $E_{AI}=17$ K for the AI process. The resulting heating rate $\dot{T}_{sec}$ of the total population of trapped atoms is given for a depth $\mathcal{E}=10$ mK of the magnetic trap. Both the high-density–low-aspect-ratio and the low-density–high-aspect-ratio cases of the final state are investigated.

	$He(^1S_0)+He^*$ PI, $E_{PI}=500$ K	$He^+ +He^*$ PI, $E_{PI}=500$ K	$He_2^+ +He^*$ AI, $E_{AI}=17$ K
s	6	4	4
$\alpha_1(s)$	0.9975		
$\alpha_2(s)$	0.2846	0.1920	0.1920
$\alpha_3(s)$	8.083	11.37	11.37
C_s (a.u.) [a]	21.82	157.8	157.8
μ (a.u.)	2	2	2.66
v (m/s)	1442	1442	373
k (a_0^{-1})	2.41	2.41	
Q_{sec} (a_0^2)	5.20×10^2	4.40×10^4	1.08×10^5
$\sigma_{sec}(0)(a_0^2)$	1.52×10^4	2.84×10^8	2.05×10^8
$\theta_{0,sec}$ (mrad)	64	7.0	13
$\theta_{max}/\theta_{0,sec}$	1.4×10^{-1}	1.3	2.0
$\Delta Q_{sec}/Q_{sec}$	7.4×10^{-3}		
$\Delta E(\theta_0)$ (mK)		6.1	2.5
$\dot{T}_{sec}$ $(\mu K/s)$ [b,c]	$0.02\,\eta_{PI}$	$91\times\eta_{PI}$	$179\times\eta_{AI}$
$\dot{T}_{sec}$ $(\mu K/s)$ [b,d]	$0.0002\times\eta_{PI}$	$1.1\times\eta_{PI}$	$2.1\times\eta_{AI}$

[a]See Ref. [46].
[b]See Table I for density, aspect ratio, and ionization decay time.
[c]High density case with $T_C=8.6$ μK.
[d]Low density case with $T_C=2.9$ μK

95 μK/s (assuming $\eta_{AI}=0.05$), which should be compared to $T_C=8.6$ μK and $\tau_i=1$ s. It is clear that this does not lead to BEC. For the low density case the conclusion is positive: the total heating rate is 1.2 μK/s at a transition temperature $T_C=2.9$ μK. When sufficiently high loading rates can be achieved to obtain an initial population of the trap of 10^9 to 10^{10} atoms, reaching BEC seems feasible. Looking at the heating rates, we can also decide on choosing for a smaller value of the transition temperature, e.g., $T_C=0.5$ μK, with a factor 13 lower demand on the number density. With the number of trapped atoms $>10^8$ the chance of success is high. This would be an important milestone in the field of BEC related physics.

Finally, we have also investigated the heating rates for the situation at the transition temperature T_C when the evaporative cooling is not switched off. The trap depth is then limited to $\mathcal{E}=6k_BT_C$, reducing the heating rates considerably. In Table III the resulting values of the heating lifetime τ_{heat} $=T_C/\dot{T}$ are given. We observe the same trend as for neon: the lifetime for heating τ_{heat} typically is a factor 4 to 10 larger than the lifetime for ionization, both for the high density and the low density case.

The UV photon emitted by the radiative decay of triplet metastable helium has an energy of 19.6 eV, corresponding to a wavelength of 56 nm. The recoil kick of the photon results in an energy transfer $E_{uv}=1.11$ mK, i.e., a velocity of 2.2 m/s. The upper limit of the heating rate is then equal to

$\dot{T}=0.04$ μK/s, which is a factor 20 smaller than for neon due to the much longer lifetime of the triplet metastable state of helium. With the same assumption for the $He(^1S_0)$ $+He(|1,1\rangle)$ scattering length as for neon (Sec. V), the heating rates are given in Table IV for the two final state geometries. Compared to the heating rate for ion–metastable-atom collisions, this contribution is negligible. Collisional heating is clearly the most important factor.

IX. CONCLUDING REMARKS

Metastable neon is an ideal gas for efficient handling of beams and traps of cold atoms. It is the equivalent of Na in many respects. The good suppression of ionization of a spin-polarized sample opens the road to BEC. Compared to the alkali's, the metastable atoms have the advantage of excellent real-time diagnostics of the trapped dilute gas, due to the UV photons and ions released by radiative decay and residual ionization, respectively. The associated side effect of heating of the trapped metastable atoms by collisions with hot (dimer) ions resulting from residual ionization can be controlled by a careful design of the trap. By choosing a trap geometry with a tight radial confinement and a depth in the 10 mK range, both the probablity for a secondary collision and the energy transferred in small angle scattering are limited to acceptable values. Typical lifetimes of the trapped sample are 1 s. Keeping the evaporative cooling switched on

after BEC has been reached results in an extension of the condensate lifetime to the ionization lifetime of five seconds.

The succes of evaporative cooling is determined by the magnitude of the scattering length $a_{2,2}$ for metastable-atom–metastable-atom collisions. As yet, no information is available on its actual value. For the upper limit $(\mathcal{K}_i^{pol})_{max} = 10^{-14}$ cm^3 s^{-1} for the ionization rate constant used throughout this paper, a scattering length $a_{2,2} \geqslant 50a_0$ is required to remain in the regime of runaway cooling. The actual lower limit for $a_{2,2}$ is determined by the actual value of the ionization rate constant for a polarized gas of metastable atoms. This is one of the first data that have to be measured in a magnetically trapped sample of atoms, using the diagnostics described in this paper. The ^{22}Ne isotope, with its 10% natural abundance, serves as a rain check when the ^{20}Ne isotope fails to meet the requirements. Bright beams of the ^{22}Ne isotope are readily produced, with a factor five loss of intensity as the only difference.

All the calculations in this paper have been made using an upper limit for the rate constant of ionization of a polarized gas, i.e., represent a worst case scenario. The chances for more favorable conditions, i.e., a smaller residual ionization rate, are large.

For metastable helium the prospects for reaching BEC are favorable. At the same density, the larger DeBroglie wavelength relaxes the demand on the final temperature. The calculated heating rates are slightly larger than for metastable neon, due to the larger value of the charge-induced dipole interaction. The major difference with metastable neon is the demand for a stronger radial gradient of the trapping field of

the magnetic trap, to obtain the same confinement with a smaller magnetic moment $\mu = 2\mu_B$.

Of the heavy rare gases Ar* through Xe*, the suppression of ionization is less efficient due to their larger anisotropy of the quadrupole-quadrupole interaction of the core hole [6]. Experiments with these species are limited to an investigation of cold collisions in magnetic traps, still yielding a rich field of physics [16]. Experiments as photoassociative ionization and Penning ionization in spin-aligned states can reveal interesting details on the ''dimer'' potentials of the metastable states. These experiments can also still open the door to BEC for metastable argon. The currently available best value for the suppression is a factor 10^3. When nature helps us, this can perhaps be improved by a factor 2 or 3, opening the road to low temperature traps and possibly BEC.

[1] M. Anderson *et al.*, Science **269**, 198 (1995).

[2] K. Davis *et al.*, Phys. Rev. Lett. **75**, 3969 (1995).

[3] C. Bradley, C. Sackett, J. Tollet, and R. Hulet, Phys. Rev. Lett. **75**, 1687 (1995).

[4] T. Killian *et al.*, Phys. Rev. Lett. **81**, 3807 (1998).

[5] D. Fried *et al.*, Phys. Rev. Lett. **81**, 3811 (1998).

[6] M. Doery *et al.*, Phys. Rev. A **58**, 3673 (1998).

[7] H. Mastwijk, J. Thomson, P. van der Straten, and A. Niehaus, Phys. Rev. Lett. **80**, 5516 (1998).

[8] C. Orzel *et al.*, Phys. Rev. A **59**, 1926 (1999).

[9] M. Müller *et al.*, Z. Phys. D: At., Mol. Clusters **21**, 89 (1991).

[10] G. Shlyapnikov, J. Walraven, U. Rahmanov, and M. Reynolds, Phys. Rev. Lett. **73**, 3247 (1994).

[11] P. Fedichev, M. Reynolds, U. Rahmanov, and G. Shliapnikov, Phys. Rev. A **53**, 1447 (1996).

[12] W. Rooijakkers, W. Hogervorst, and W. Vassen, Opt. Commun. **135**, 149 (1997).

[13] W. Vassen, in *Ultra-cold atoms and Bose-Einstein Condensation*, Vol. 7 of *Trends in Optics and Photonics*, edited by K. Burnett (Optical Society of America, Washington, DC, 1996), p. 20.

[14] N. Small-Warren and L. Chin, Phys. Rev. A **11**, 1777 (1975).

[15] M. Walhout, A. Witte, and S. Rolston, Phys. Rev. Lett. **72**, 2843 (1994).

[16] M. Doery *et al.*, Phys. Rev. A **57**, 3603 (1998).

[17] J. Lawall, C. Orzel, and S. Rolston, Phys. Rev. Lett. **80**, 480 (1998).

[18] D. Jaksch *et al.*, Phys. Rev. Lett. **81**, 3108 (1998).

[19] M.-O. Mewes *et al.*, Phys. Rev. Lett. **77**, 416 (1996).

[20] J. Walraven, in *Quantum Dynamics of Simple Systems*, Vol. 44 of *Scottish Universities Summer Schools in Physics Proceedings*, edited by G.-L. Oppo, S. Barnett, E. Riis, and M. Wilinson (Institute of Physics, Bristol, 1996), p. 315.

[21] W. Ketterle and N. van Druten, *Advances in At. Mol. Opt. Phys.*, edited by B. Bederson and H. Walther (Academic Press, New York, 1996), Vol. 37, p. 181.

[22] A. Niehaus, in *The Excited State in Chemical Physics*, Vol. 45 of *Advances in Chemical Physics*, edited by J. W. McGowan (Wiley, New York, 1981), Pt. 2, p. 399.

[23] S. Kotochigova, E. Tiesinga, and I. Tupitsyn (unpublished).

[24] J. Driessen *et al.*, Phys. Rev. A **44**, 167 (1991).

[25] S. Op de Beek, J. Driessen, H. Beijerinck, and B. Verhaar, Phys. Rev. A **56**, 2792 (1997).

[26] S. Op de Beek, J. Driessen, H. Beijerinck, and B. Verhaar, J. Chem. Phys. **106**, 1 (1997).

[27] K. Ford and J. Wheeler, Ann. Phys. (N.Y.) **7**, 259 (1959).

[28] K. Ford and J. Wheeler, Ann. Phys. (N.Y.) **7**, 287 (1959).

[29] H. Pauly, *Physical Chemistry*, edited by W. Jost (Academic, New York, 1975), Vol. 6B, p. 553.

[30] D. Beck, in *Molecular Beams and Reaction Kinetics*, edited by

C. Schlier (Academic, New York, 1970), p. 15.

[31] H. Beijerinck, P. van der Kam, W. Thijssen, and N. Verster, Chem. Phys. **45**, 225 (1980).

[32] E. Mason, J. Vanderslice, and C. Raw, J. Chem. Phys. **40**, 2153 (1964).

[33] L. Schiff, Phys. Rev. **103**, 443 (1956).

[34] L. Landau and E. Lifchitz, *Quantum Mechanics* (Pergamon Press, London, 1959), p. 146.

[35] R. Molof, H. Schwartz, T. Miller, and B. Bederson, Phys. Rev. A **10**, 1131 (1974).

[36] J. Cohen and B. Schneider, J. Chem. Phys. **61**, 3230 (1974).

[37] E. Vredenbregt, K. van Leeuwen, and H. Beijerinck, Opt. Commun. **147**, 375 (1998).

[38] M. Hoogerland *et al.*, Appl. Phys. B: Lasers Opt. **62**, 323 (1994).

[39] K. van Leeuwen *et al.*, in *The Physics of Electronic and Atomic Collisions: XIX International Conference*, Whistler, Canada, 1995, edited by L. J. Dube *et al.*, AIP Conf. Proc. No. 360 (AIP, Woodbury, 1996), p. 731.

[40] W. Rooijakkers, W. Hogervorst, and W. Vassen, Opt. Commun. **123**, 321 (1996).

[41] H. Mastwijk, Ph.D. thesis, University Utrecht, 1997.

[42] M. Hoogerland *et al.*, Aust. J. Phys. **49**, 567 (1996).

[43] F. Dalfovo, S. Giorgini, L. Pitaevski, and S. Stringari, Rev. Mod. Phys. **71**, 463 (1999).

[44] T. Bergeman, G. Erez, and H. Metcalf, Phys. Rev. A **35**, 1535 (1987).

[45] J. Woodworth and H. Warren, Phys. Rev. A **12**, 2455 (1975).

[46] D. Spelsberg and W. Meyer, J. Chem. Phys. **99**, 8351 (1993).